

Chapter 1

Imaging

In this thesis, we have imaged two galaxies- IC 342 and NGC 628, using the HBA data.

1.1 NGC 628

NGC 628 is an almost face-on grand design late-type spiral galaxy. It is located at a distance of almost 7.3 Mpc (?). Details on the galaxy can be found in the Table 1.1. It has two clearly defined spiral arms that can be seen in any optical image of the galaxy. In the UV, the spiral arms can be seen as bright knots on diffuse emission (?), and these knots are also traced in the H α . It is an isolated galaxy, and does not have strong density waves. HI holes have been detected in the HI layer of the galaxy, with sizes ranging from 0.24 kpc to 2 kpc ?. The galaxy is seen to consist of two disks, the inner disk being 8-10 kpc. These regions span different type of stellar populations ?, with a colder inner region ?, and faint H II regions covering the outer part of the galaxy (?). The H I distribution is seen to be extended and asymmetric to the southwest. In ?, it was seen that the inner part of the galaxy has a flat differentially rotating disk while the outer part is not a “well-behaved” disk. In ? it was concluded that the inner part of the galaxy has no dust lanes, while outer part of the galaxy has clear nuclear dust spirals.

Distance ¹	~7.3 Mpc
Position ²	RA:01h36m41.74s DEC:+15d47m01.1s
Morphology ³	SA(s)c
Star Formation Rate ⁴	1.21 M_{\odot} /year
Inclination angle- inner disk (deg) ⁵	7
Inclination angle- outer disk (deg) ⁶	13.5
Position angle (deg) ⁷	02

Table 1.1: Parameters of NGC 628

1.2 IC 342

IC 342 is an intermediate, almost face-on spiral galaxy of the Maffei 1/IC 342 group, the galaxy group nearest to our Local group, at a distance of around 3.3 Mpc(?). Details on the galaxy can be found in the Table 1.2. There has been a great amount of interest in the study of the galaxy, as it has a structure most similar to our own galaxy with similar dynamical mass ($2 \times 10^8 M_{\odot}$) (?). The super massive black hole mass at the center of IC 342 is also of the same order ($\sim 10^6 M_{\odot}$) as Milky Way. It is only 10.6 deg above the galactic plane, and is not clearly visible because of the Galactic disk and the large number of foreground stars in optical regime. It is the third largest spiral galaxy in the sky, with an angular size of . It consists of a central nuclear star cluster, where a lot of the star formation occurs. There exist five prominent Giant Molecular Clouds (GMCs) in the molecular ring and the arms, each of the mass of approximately $10^6 M_{\odot}$ (?). The nucleus of the galaxy consists of two mini-spiral arms that are connected to the inner molecular ring. This structure is seen due to the presence of barred potential,

Position ⁹	RA:03h46m48.503s DEC:+68d05m46.92s
Distance ¹⁰	~3.3 Mpc
Morphology ¹¹	SAB(rs)cd
Star Formation Rate ¹²	2.8 M_{\odot} /year
Inclination angle (deg) ¹³	30
Position angle (deg) ¹⁴	39.4
B _T (mag) ¹⁵	9.16

Table 1.2: Parameters of IC 342

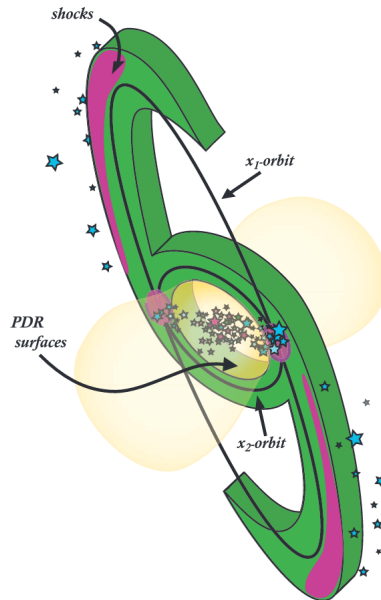


Figure 1.1: Schematic of the chemical and physical structure of the nucleus of IC 342(?)

which is also indicated by the morphology of the velocity residuals⁸ which showed the presence of a large bipolar structure (?). The outer part of the galaxy can be seen to have four distinct arms, with the inner part having speeds up to $38 \pm 7 \text{ km s}^{-1}\text{kpc}^{-1}$ and the outer part ($\sim 5 \text{ kpc}$ from center) having a speed of around $11 \pm 6 \text{ km s}^{-1}\text{kpc}^{-1}$ (?). Photo-dissociation Region (PDR) is present within the central 400 pc of IC 342 (?). The physical and chemical geometry can be best understood from diagram 1.1 of IC 342. The yellow regions represent the H II regions. The star formation in the nuclear region was studied using Radio Recombination Lines (RRLs) and continuum emission at C-band and Ka-band with the JVLA, and two components were resolved lying east and west of the central star cluster, which were associated with two GMCs. It was predicted that several compact H II regions provide best fit for the two regions (?). It is at a low inclination of 31 deg, according to the HI kinematic data, which also indicates the counter-clockwise rotation of the galaxy (?), assuming trailing spiral arms. With the help of H II and S II filters, 16 Supernova Remnants were identified, most of them being near or in the H II regions and two of them isolated (?). IC 342 is also the host of four Ultra Luminous X-ray sources (ULX) (?).

Being an axis symmetric spiral (ASS), over the years, magnetic fields in this galaxy have been studied at several wavelengths- 6.2 and 11 cm (?), at 20 cm (?). Recently, Faraday tomography of the local ISM with LOFAR, in (?), showed the presence of two Faraday thin neutral clouds clearly separated in Faraday depth. In this thesis, we have also studied the polarized sources in the field of view of the galaxy at frequencies as low as 150 MHz. More information about the magnetic fields in IC 342 can be found in section “Magnetic fields” chapter.

⁸Subtracting the the rotation model with the observed velocities gives the residual velocities

1.3 Observational setup

NGC 628: The observations for NGC 628 were done in an interleaved mode. The calibrator used was 3C 48, and the scans were alternatively taken from the target to the calibrator. The observation used 14 remote stations and 23 core stations. The number of stations used for the observation of NGC 628 was 37. No international stations were used. Details of the observation can be found in the table 1.3. The baselines used for the observation can be seen in Figure 1.2 that shows the UV distance in meters and amplitude plot.

Start date (UTC)	22-Nov-2013 / 15:19:00.0
End date (UTC)	23-Nov-2013 / 00:50:59.9
Interleaved calibrator	3C48
Scan length on calibrator	2 min
Scan length on target	20 min
Duration of observation	9 hours 32 min
Final time on target	8 hours (24 scans)
Frequency range (from Pre-factor)	110.667-179.027 MHz
Frequency range (for Factor)	110.667-169.239 MHz
Total bandwidth on target	68.36 MHz
Final bandwidth in target	58.57 MHz

Table 1.3: Parameters of NGC 628

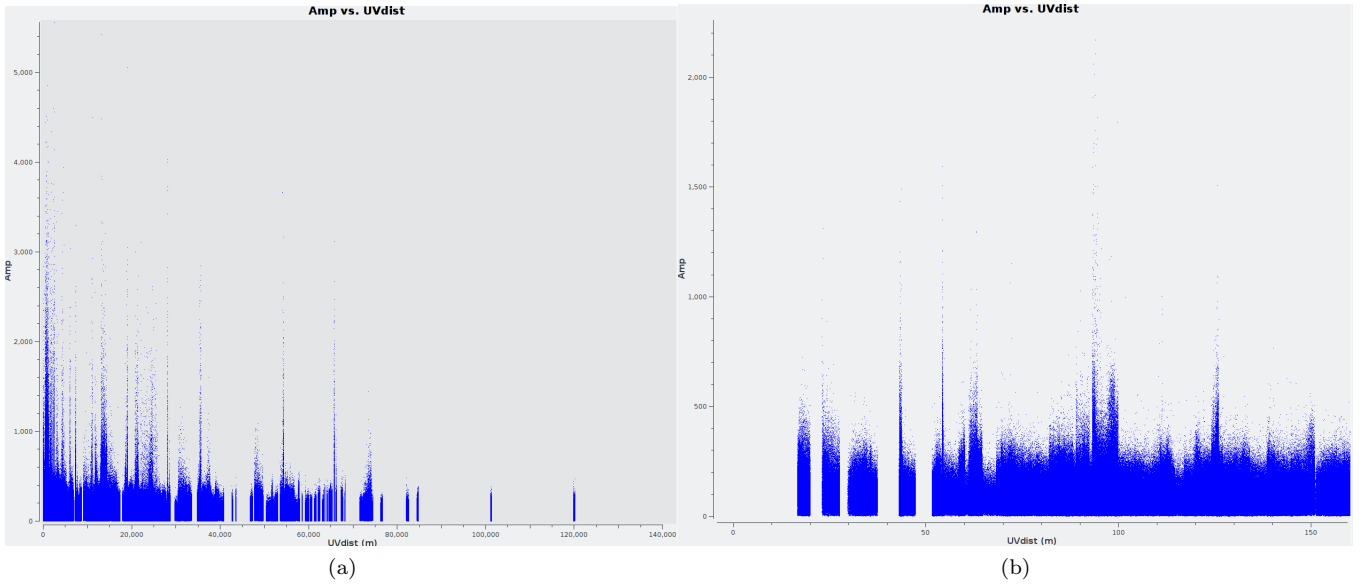


Figure 1.2: This was the arrangement of baselines used for the observation. This is a plot generated by task in CASA called 'plotms' for the first measurement set for the frequency 111 MHz in the first time step. From the plot, one can see the baselines used in terms of meters. As can be seen, the observation uses a dense core to image diffuse flux in the galaxy-the disk and the halo parts. *Right:* This image shows the shorter baselines used. The shortest projected baseline used was around 23 m.

1.4 Calibration of LOFAR data

Calibration in LOFAR is especially difficult due to the ionosphere that causes delay differences between antenna stations. This gives rise to additional phase errors in the visibilities that vary station to station due to LOFAR's large array size. This phase depends on two factors: (1) Free electron column density along the line of sight, (2) Frequency being observed. Another aspect to be noted while calibration of LOFAR is the station beam shape that varies with time and also, the difference between the beam model and the actual beam shape.

In order to take care of these effects, LOFAR data calibration involves two major parts. In this thesis, a tool called Factor¹⁶ was used. The major steps to the data reduction are explained below. An overview on how to use the tool itself is described in a later section 1.4.3.

1.4.1 Direction independent part

The first step to do direction independent calibration is the flagging of RFI (Radio Frequency Interference) with the help of `AOFlagger` (?). Then, the data is averaged using `NDPPP` to be 4s in time resolution and 4 channels per sub-band in frequency resolution, to reduce the size of the data. Then, all baselines with CS013 HBA station were flagged and a flux density scale was created for 3C 48 (which was chosen as the amplitude calibrator source) using the model that shows the flux density values of the source at several different frequencies, with a flux density of 64.76 Jy at 150 MHz, as described in ?. Using this primary beam calibrator, the gain solutions are obtained using `BlackBoard Selfcal` (BBS) for all four correlations. The gain solutions are then transferred to the target(?) data to correct for the instrumental effects¹⁷. The A team sources affect the visibilities through the side lobes of the station beam. Hence, the visibilities in which the contribution is more than 5 Jy (in apparent flux density) are flagged. This was followed by another round of flagging, and averaging. The data was concatenated into subbands with time resolution of 8 s. The width of each channel was kept at 48.828 kHz, and the total bandwidth was at 1.95 MHz. The last step in direction independent calibration involves the subtraction of sources by first subtracting clean components in medium resolution images, and then re-imaging the subtracted image at a lower resolution (1.5' and uv cut range of 2 kλ) and full field of view image [write dimensions here]. This is done in order to detect the extended flux emission and sources in the first and second side lobes. The new components found using the lower resolution image were again subtracted from the obtained visibilities. The clean components obtained from the two imaging steps in the direction independent part of calibration are convolved with the gain solutions and subtracted from the uncorrected visibilities and the obtained visibilities were used as input for the direction dependent calibration. Sky models for each frequency were generated (to take care of frequency dependence) which would be used in the later steps of factor.

1.4.2 Direction dependent part

From the Figure 1.6, it can be seen that the artifacts from brighter sources severely affects the image quality. Hence, in order to reduce the noise in the image due to ionosphere and the station beam effects, “faceting” is done obtain solutions and reach near-thermal noise limited images. The field of view is divided into a number of small isoplanatic patches called facets. We assume that the calibration solution towards the brightest source in the facet can be used for the facet as a whole.

For NGC 628: The visibilities obtained from prefactor were moved to the lofar4 cluster where the direction dependent calibration was to be done. The frequencies above 170 MHz were not taken for the next part, as they seemed to have bad visibilities. The first time step was also removed owing to corrupted visibilities. The first step to do DDE calibration is to make a list of the sources to make facets around. The sources above 100 mJy in

¹⁶<https://github.com/lofar-astron/factor>

¹⁷**Instrumental effects:** The clocks at the remote stations are not perfectly synchronized, which causes a phase delay. This in addition to the phase delay by the ionosphere gives rise to phase errors. The phase difference for a baselines can be written as:

$$\Delta \text{ phase}(\nu, t) = \underbrace{2\pi p_0(t)\nu}_{\text{Clock difference effects}} - \underbrace{\frac{8.448 \times 10^9 p_1(t)}{\nu}}_{\text{Total Electron Content (TES) effects}} \quad [\text{rad}]$$

Here ν represents frequency and p_0 and p_1 represents the clock difference and TEC difference. These errors need to be removed. This is done with the help of a bright source with a high Signal to Noise ratio on all baselines. Brute force search is done to obtain clock and TEC initial guesses, as computing using the equation is not computationally feasible.

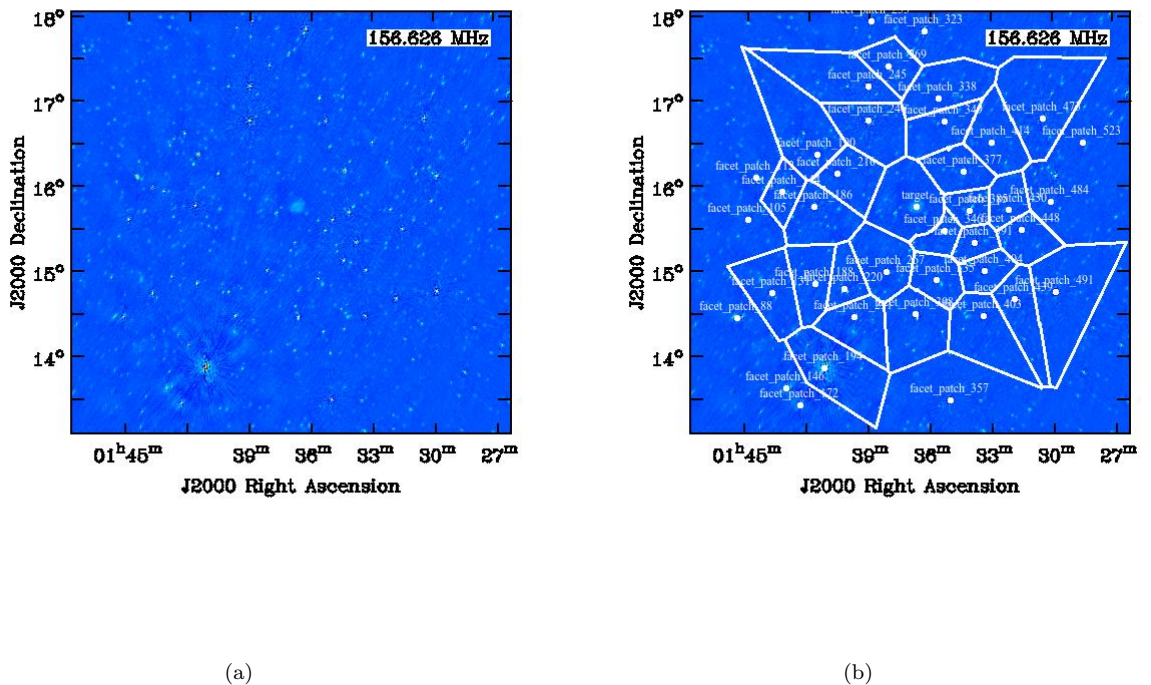


Figure 1.3: *Left:* Initial subtract image of NGC 628, using frequencies between 135 to 167 MHz. It has a restoring beam of 43.99 arcsec by 31.64 arcsec and position angle of -17.27deg. As can be seen, artifacts from individual sources, such as 3C 049 (at RA: 01h41m09.160s and DEC: +13d53m28.05s in J2000 coordinate system), can severely affect the galaxy image quality. Hence, the field of view is divided into “isoplantic” patches called “facets”. *Right:* The facet patches can be seen in the image, and are made around the radio sources present in each facet. They are represented by the white dots in the image on the right. The facet patches are based on the Veroni tessellation scheme.

apparent flux density were selected, with maximum size of $2.0'$. They were set to be separated by a distance of at least $7'$. In cases where more than one source was used as calibrators, the collective maximum flux was set to be 100 mJy. The faceting was done upto a radius of 2.8 deg^{18} . If any sources were found at a higher radius than that, a small patch was made around this part. One such source was 3C 047, a quasar, which is labeled as source 1 in the Figure 1.4. The boundaries for some of the sources had to be changed¹⁹ to get better self calibration results (to remove the secondary sources in the facet). The calibration begin with source 194- commonly known as 3C49. The self-cal images after each iteration of 3C49 is shown in Figure 1.5. To do the self- calibration, the source is first added back to the visibility data (the residual visibility obtained from DIE calibration), and phase shifted to the source in the facet, which in the fist case was 3C 49. This is followed by the “short-timescale phase +TEC” calibration to take care of the ionospheric delay (row 2 in the Figure 1.5). Then, to take the effects of the slowly varying station beam into account, the “slow gain” calibration is done. Then the imaging of the facet is done. Once the DDE calibration solutions for the facet are obtained, the other fainter sources within the facets are added back and corrected using the solutions of the strongest source that was used for the calibration. This is followed by the generation of an updated skymodel which is then subtracted from the residual visibilities with the obtained solutions. This whole process is then repeated for another facet that has the source with next highest flux density, so that the sources that have a higher calibration errors do not affect the DDE calibration of the fainter sources in other facets.

For IC 342: The Figure 1.7 shows the facets on the field of view of the observation, and the different directions in which the faceting was done. The sources above 300 mJy in apparent flux density were selected, with maximum size of $2.0'$. They were set to be separated by a distance of at least $7'$. In cases where more than one source was used as calibrators, the collective maximum flux was set to be 200 mJy. The faceting was done upto a radius of 1 deg , while the sources for the directions were set to be searched up to $7'$. A directions file was made by factor based on the given parameters. Then, a few changes were made²⁰ The rest of the procedure followed was mimicking the one for NGC 628.

1.4.3 Overview of Factor

This section gives the description of the steps to calibrate LOFAR data with the help of Factor. Imaging, for both IC 342 and NGC 628 was done on interleaved data-sets. Factor is used to produce deep images using the HBA data employing the direction dependent facet calibration method as described in (?). The first step to calibration, involves the preparation of the data, using a tool called Pre-factor²¹, which also does the **Direction independent calibration**.

Step 1: The data of the calibrator and target are kept in separate directories. The calibrator data is first processed using the Calibrator Pipeline. The gain solutions obtained using the calibrator are then used for the clock-TEC separation and to compute average gain amplitudes.

Step 2: The target data processing is done. This uses the Target Pipeline that adds the Rotation Measure correction from RMextract to the data file (h5parms) from the Calibrator Pipeline. This requires files that contain information about the ionospheric electron content. It also pre-process the input measurement sets (MSs) and applies the values from the h5parms. It predicts and flags the A-team contamination, and sorts the MSs by time and frequency into groups that are later concatenated. It removes the files with too much flagged data. It also does phase-only calibration on the skymodel. It also produces diagnostic plots, that can be seen in the table 1.4.
Step 3: The final part of Pre-factor is the “Initial subtract” pipeline that produces the sky-model required for Factor from the visibilities. Initial- subtract also gives the full field of view image. In our analysis, raw data was used (non-NDPPP-ed data: no demixing, averaging and flagging was done before-hand), which required the “Pre-Facet-Calibrator-RawSingle” parset (this option is not available in Prefactor anymore). The target part of the calibration was done in six batches due to the large size.

Once the data has been prepared using Prefactor, the **Direction Dependent calibration** is done.

Step 1: The Factor parset is prepared. In this, one can specify any additional flagging needed. One can also give instructions on the field in which faceting needs to be done, and the maximum size of facets and soures (or group

¹⁸This is by default at a value of $\frac{FWHM \times 1.25}{2}$ of the primary beam at the highest frequency.

¹⁹Sources 246, 385, 335, 349, 267, 253, 477, 144

²⁰The boundaries for some of the sources had to be changed to get better self calibration results (to remove the secondary sources in the facet). A few of the sources below the given flux density limit had to be given their own facets. There sources were marked with the prefix ‘d’, see Figure 1.7

²¹<https://github.com/lofar-astron/prefactor/wiki>

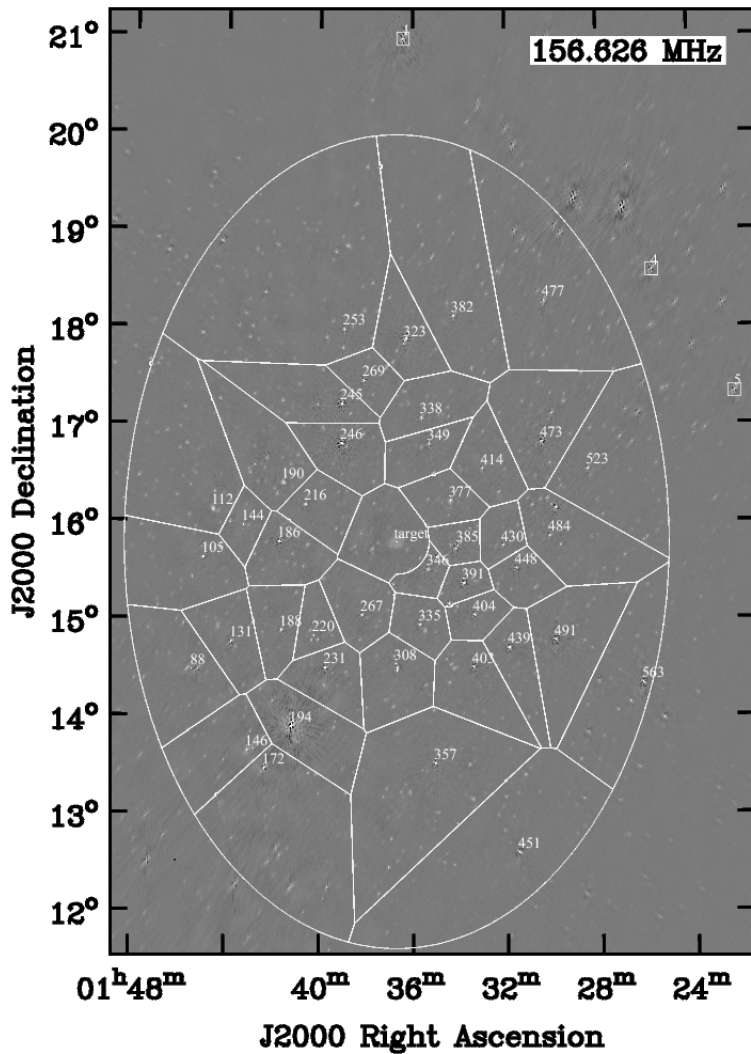


Figure 1.4: This image depicts the faceting scheme used for NGC 628. The middle facet marked “target” is NGC 628. The sources marked 1, 4 and 5 were included by hand due to their high fluxes. The image is the one obtained from the initial calibration (same as the one in the previous figure). The beam is elongated to account for the low elevation elongation of the LOFAR primary beam.

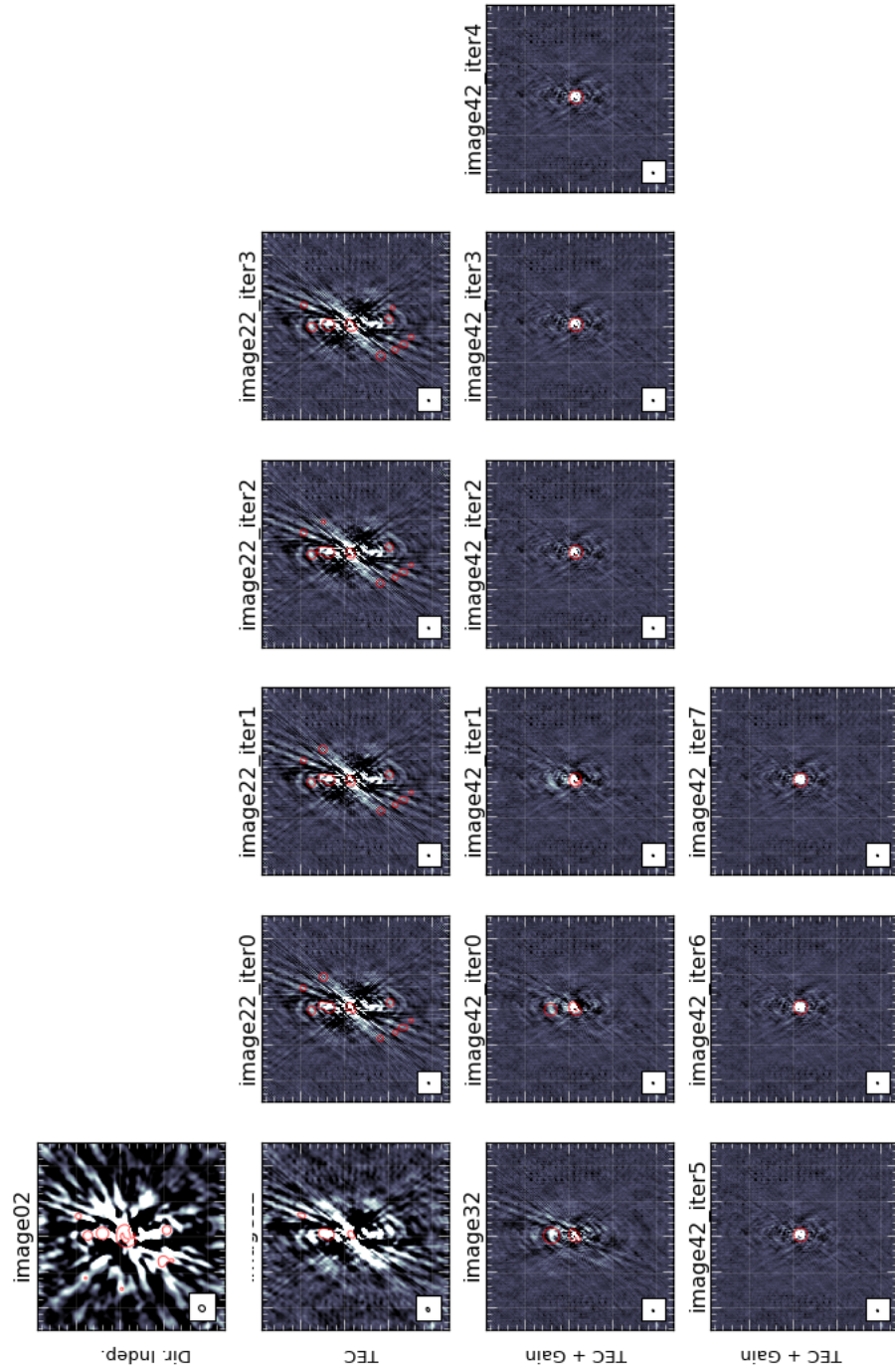


Figure 1.5: Self calibration images of the facet with source 194- otherwise known as 3C49. The image marked “Dir. Indep.” is the direction independent image of the facet. In the second row, the phase term is being solved, which took three iterations. Then, the phase + amplitude calibration was done, which took 7 iterations.

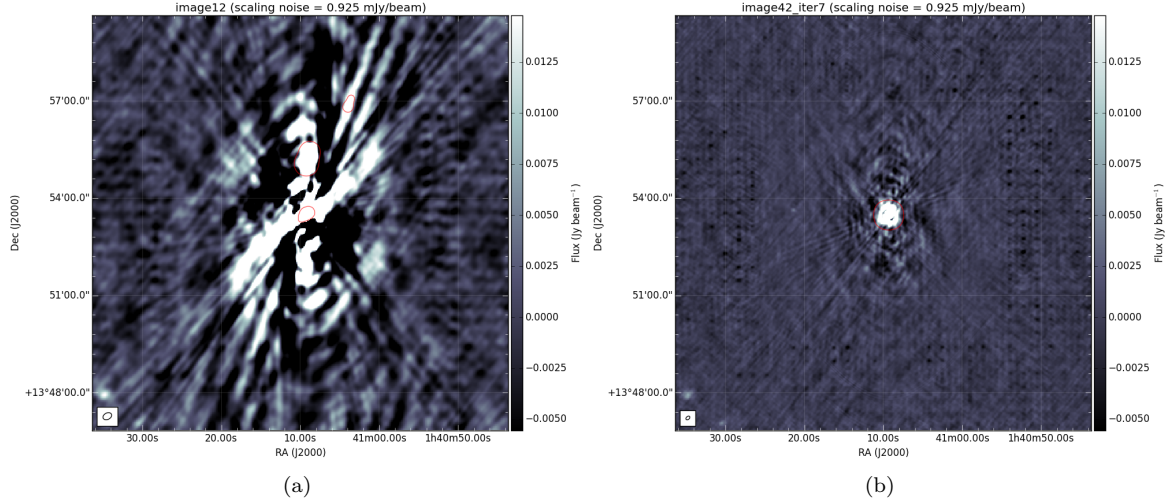


Figure 1.6: *Left:*The initial subtract image of facet containing the source 3C49. *Right:*Final self-cal image of 3C49. The image is considerably better than the one on the left, however some of the artifacts still remain. The source is the source is farther away from the target source, hence, the artifacts that remain do not affect the image too much.

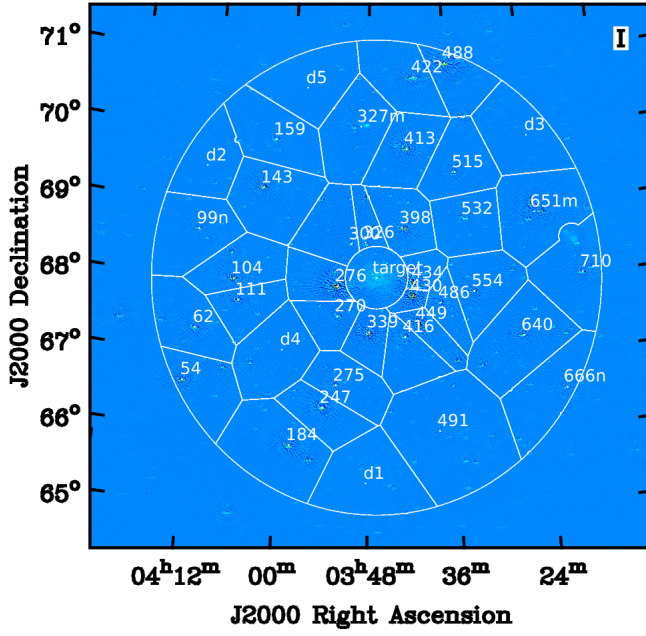
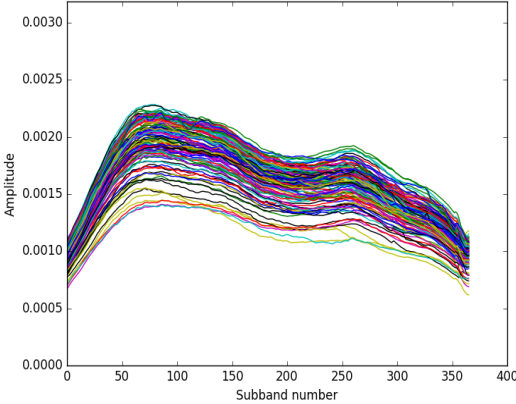
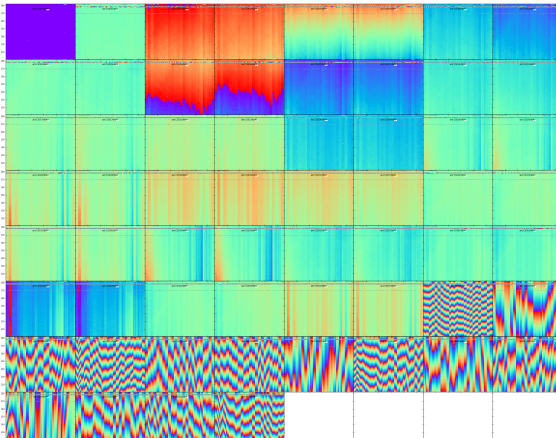
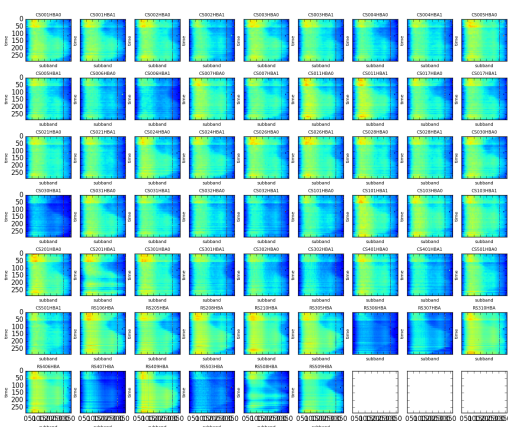


Figure 1.7: Faceting in IC 342 for Direction Dependent calibration in Factor. The facets have been overlaid on the image made using averaged Prefactor data. The resolution of the image is 17.35 by 12.72 arcsec. It was cleaned to a threshold of 0.3 mJy with Briggs weighting of -0.5.

of sources).

Step 2: The directions file can either be generated by Factor, or be edited by the user. One may also remove some of the directions, and add a few depending on what is needed. Factor is run using the command “runfactor”.

Step 3: One can check the progress of the Factor run, with the help of the command “checkfactor”. In Factor, various operations are simultaneously undertaken: Outliers and sources in each of the facets are peeled in the operations named “outlierpeel” and “facetpeel” respectively. This is followed by “facetselfcal” which self calibrates the facet calibrator. “facetsub” operation subtracts the model of the facet and calibrator. The imaging of the facet is done in the “facetimage” operation, in which the facet is imaged using full bandwidth, unlike in the “facetselfcal”, in which only part of the bandwidth is used to image the facet. If the full field of view image is required, it can be done using the “fieldmosaic” operation, in which all the final facet images are made into a mosaic, after the primary beam attenuation correction. The main output of Factor is generated in the “results” directory, which contains the self-calibrated visibilities and the self-calibrated images of the different facets.

Diagnostic plots	Description
	This graph shows the amplitude solutions in the different subbands. As can be seen, there are no clear outliers, showing that this data set does not have bad amplitude solutions.
	This plot shows the calibrator solutions in the YY polarisation. The CS001HBA0 station is flagged, and some of the frequencies between 170 to 180 MHz seem to have noisy data.
	This shows the waterfall plots of the amplitude solutions for the single stations. It can be used to see which stations are bad in the first plot.

Diagnostic plots	Description
	This plot shows the differential Total Electron Content (dTEC). It shows that the data is fine, even though it may be noisy.
	This plot shows the differential clock values. For all the core stations, the values should lie on 0.
	This plot gives the median difference of the phase solutions for the X and the Y antennas. For the station calibration, the X and Y dipole phases are not aligned with each other resulting in phase offsets. The blue spikes represent the ones that have been flagged by pre-factor.

Table 1.4: This table shows the diagnostic plots that are obtained as an output from the Prefactor pipeline. They give an overview of the condition of the data and help us select and flag any data sets that seem bad, and were not previously flagged by the pipeline.

Weighting	Description	Notes
Natural	Constant weights to all visibilities	Lowers the noise level Good to study point sources.
Uniform	Weights are inversely proportional to sampling density function	Noise can be a factor of two larger. Lowers side lobes.
Briggs	Compromise between Natural and Uniform weighting- defined by robust parameter (-2 to +2)	Good for diffuse source imaging. Robust parameter = -2 \Rightarrow Uniform weighting Robust parameter = +2 \Rightarrow Natural weighting

Table 1.5: The weighting schemes in imaging synthesis.

1.5 Imaging

Common Astronomy Software Application²² CASA is used to make images of the two galaxies, using the visibilities of the target facet. The LOFAR primary beam is much larger than the size of the galaxies, and hence, LOFAR primary beam correction was not done. Several images have been made with various weighting schemes and taperings. CASA gives an option of the ‘Robust’, which helps us choose the required weighting scheme. There exist three weighting schemes, as given in table 1.5. For more information, one can visit <https://casa.nrao.edu/docs/casaref/imager.weight.html>.

For IC 342 : One of the major problems encountered during the imaging of IC 342 is the presence of the source at RA: 03h47m28.8s and DEC: +68d08m23s, with a flux density of around 212 mJy/beam at 145 MHz. In the NVSS survey ?, it has been defined as a radio source, as well as in the paper ?. However, it is unknown as to what this source might be.

We can rule out the possibility of the source being a supernova remnant (SNR). For example, consider the SNR Casseopeia A. If the source were an SNR, its flux density should have a similar value as that of Cas A. The flux density of Cas A at a distance of around 3.4×10^3 pc would be around 1.24×10^4 Jy for the frequency of LOFAR (?). This flux density value was obtained by extrapolating the flux density values in the NED database to 145 MHz frequency with a spectral index value of -0.93. We know that flux density scales as $\frac{1}{d^2}$, where d is the distance to the object. Hence, at that distance, the flux density of this SNR would be 0.011 Jy, much too low for the object in the image. For Crab Nebula, another SNR, this value is even lower $\sim 4.5 \times 10^{-4}$ Jy. Hence, we can conclude that this source must be a quasar or a radio galaxy. Also, there are four known SNR²³ present in the galaxy, which can be seen in the Figure 1.8 (?). None of these SNRs have a flux density as high as the one seen in the image for the source considered.

An attempt to get rid of the artifacts has been made by subtracting the source from the visibilities after obtaining them from Factor. However, there is no change from the previous attempts, as can be seen from Figure 1.9.

In the end, three images of varying resolutions are made. The noise of each image is obtained from the rms value of a region around a part of the image with no source. The images are made using the multi-scale clean technique. The Figure 1.10 is obtained using the visibilities from Factor. A brief summary of the image parameters are provided in the table 1.6. An outer tapering²⁴ of 14 arcsec by 9.5 arcsec has been applied. The image has a resolution of 12.48 arcsec by 10.26 arcsec, while the noise in the image is of the order of $390 \mu\text{Jy}/\text{beam}$. The Figure 1.11 uses the circular outer tapering of 22 arcsec. The image thus retrieved has a resolution of 25.93 arcsec by 23.26 arcsec, while the noise in the image is of the order of $560 \mu\text{Jy}/\text{beam}$. The image 1.12 uses an outer tapering of 37 arcsec. The noise in this image is of the order of $780 \mu\text{Jy}/\text{beam}$. The image has a resolution of 38.15 arcsec by 34.39 arcsec. All of these images have been made using the Briggs weighting scheme with a robust parameter of -0.5. A positive weighting scheme gave rise to peculiar artifacts in the image, and hence was avoided for this galaxy.

For NGC 628 : For NGC 628, the imaging is pretty straight forward. The target visibility data set is imaged using various weighting schemes. The galaxy is hardly visible at resolutions as high as 15 arcsec. Hence, all

²²<https://casa.nrao.edu/>

²³These SNRs have been detected by combining the images of the galaxy in H α and |S II| light. The emission nebulae have been sorted out with a low $\frac{H\alpha}{[SII]}$ line intensity ratio.

²⁴In CASA, one can provide a tapering of in the image plane by providing the FWHM. This is the kernel used to convolve the image, and thus obtain an image with the resolution similar to the measures given (in arcsec). One could also give the taper in terms of uv baselines, and these can be in kpc, or in λ , and the specified baselines would be flagged/‘tapered’ out

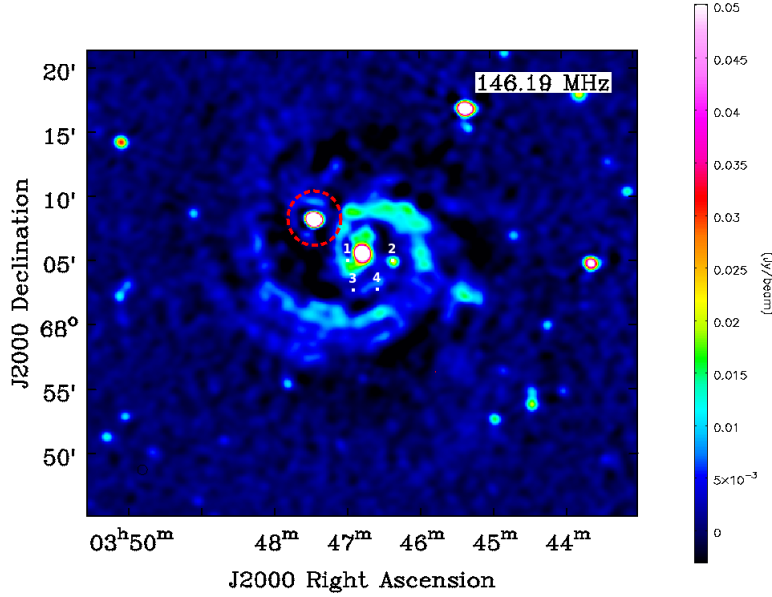


Figure 1.8: The four SNR candidates (labelled 1,2,3 and 4). The source in the dotted red circle cannot be a SNR because these SNRs do not have a flux density as high as the source.

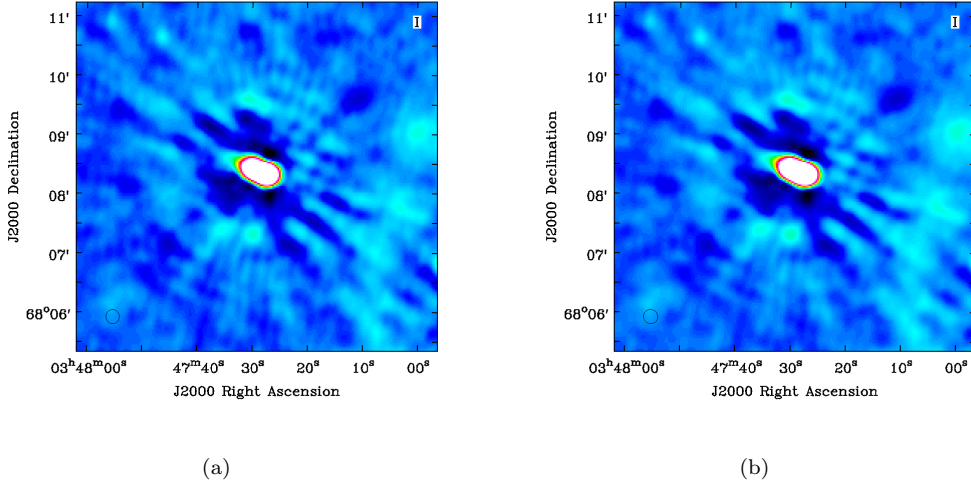


Figure 1.9: This image depicts the source that was a major problem in the imaging of IC 342, giving rise to several artifacts. The Figure on the left depicts the image in which the source has been subtracted while on the right, the source remains. There is little to no difference between the two and there is almost no change in the noise of the images. Hence, subtracting the source also provided no help.

Tapering	Robust parameter	Resolution (/beam)	Noise
14 arcsec by 9.5 arcsec	-0.5	12.48 arcsec by 10.26 arcsec	390 μ Jy
22 arcsec (circular)	-0.5	25.93 arcsec by 23.26 arcsec	560 μ Jy.
37 arcsec (circular)	-0.5	38.15 arcsec by 34.39 arcsec	780 μ Jy

Table 1.6: The parameters of the images for IC 342.

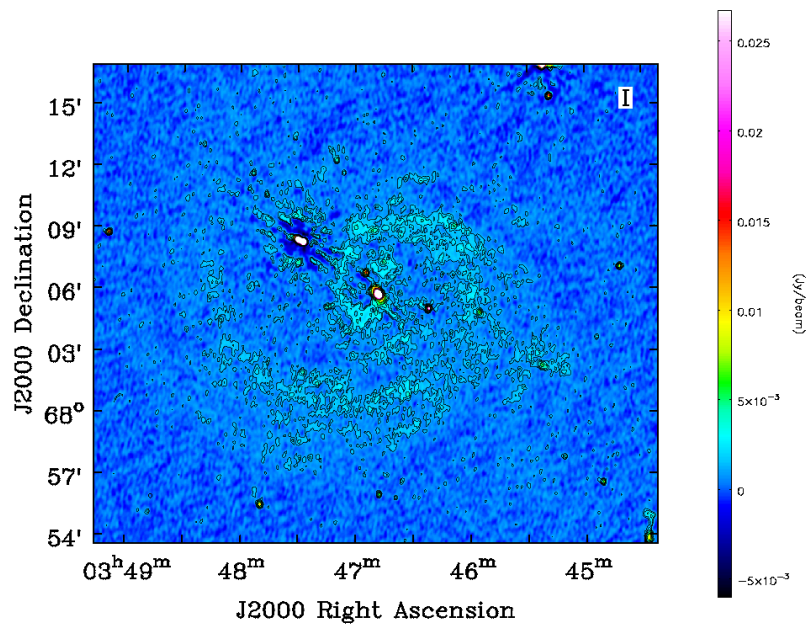


Figure 1.10: This is the LOFAR image of IC 342 at the central frequency of 146.2 MHz. Bandwidth of the observation was 62.5 MHz. This image has the resolution of 12.48" by 10.26"; PA: -8.10 deg. The contours are at 3, 8, 12, 18, 32 and 44×0.39 mJy/beam, which is the noise of the image in a quiet region.

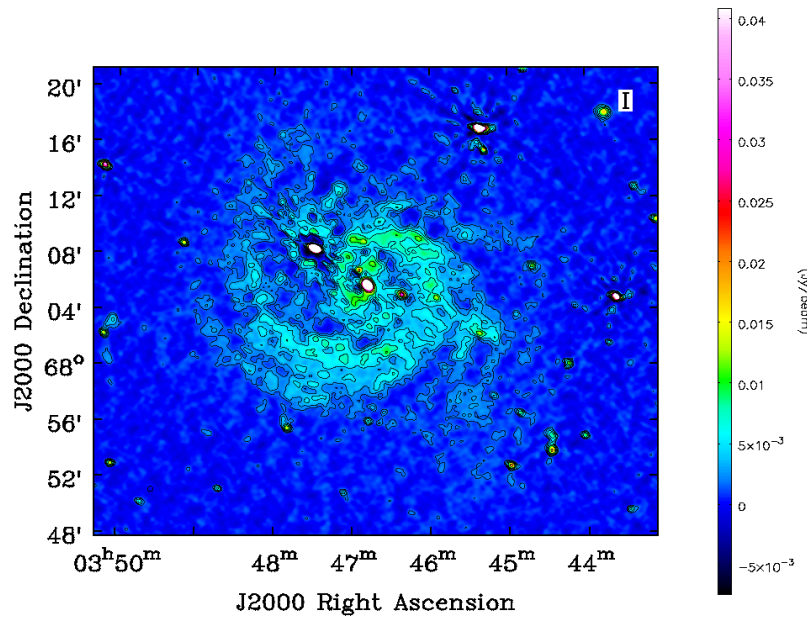


Figure 1.11: This image has the resolution of 25.93" by 23.26"; PA: 62.7 deg. The contours are at 3, 8, 12, 18, 32 and 44×0.56 mJy/beam, which is the noise level of the image.

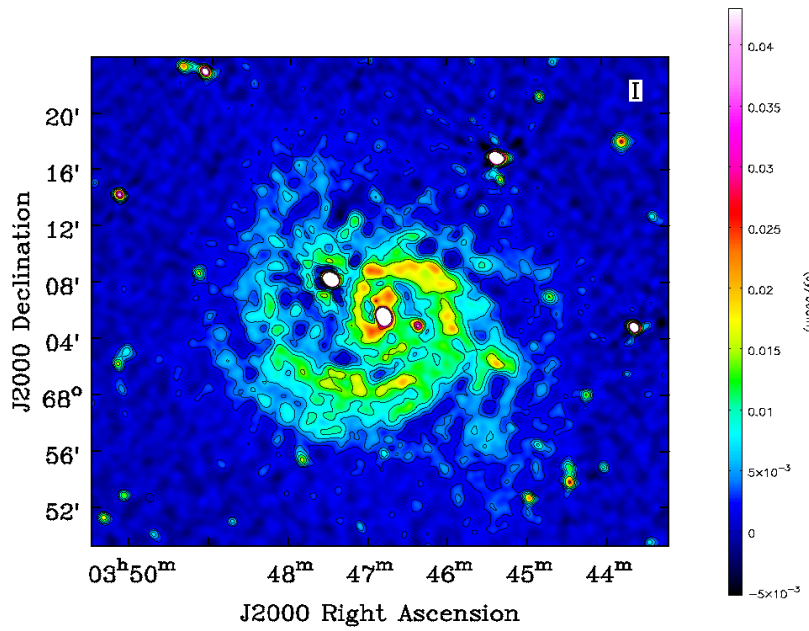


Figure 1.12: This image of IC 342 has the resolution of 38.15" by 34.39"; PA: 23.99 deg. The contours are at 3, 8, 12, 18, 32 and 44 \times 0.78 mJy/beam, which is the noise level of the image.

Tapering	Robust parameter	Resolution (/beam)	Noise
No taper	+0.5	20 arcsec	975 μ Jy
15 arcsec (circular)	-0.5	26.06 arcsec by 25.21 arcsec	1.04 mJy
35 arcsec (circular)	-0.5	40 arcsec	1.06 mJy

Table 1.7: The parameters of the images for NGC 628.

the images of the galaxy included in this thesis are of a lower resolution than that. A summary of these image parameters are given in the table 1.7. The Figure 1.13 is made using the robust weighting of +0.5. The noise in the image is of the order of 97 μ Jy/beam. The image originally made by casa with a resolution of 18.85 arcsec by 18.24 arcsec has been smoothed to a resolution of 20 arcsec with position angle of 180 deg. The Figure 1.14 is made using the robust weighting of -0.5, with an outer tapering of 15 arcsec. The resultant image has a resolution of 26.06 arcsec by 25.21 arcsec with a position angle (PA) of 88.26 deg, with the background noise of the order of 1.04 mJy/beam. The image 1.15 has been made with a Brigg's weighting of -0.5. Circular outer tapering of 35 arcsec has been used. The resultant image, with a resolution of 37.23 arcsec by 36.49 arcsec, has been smoothed to 40 arcsec with position angle of 180 deg. It has a noise level of the order of 1.06 mJy/beam. This has been made to take a look at the large scale structures.

Difference in noise level It is to be noted that the noise level of NGC 628 is much higher than that of IC 342. This may be because of several reasons, as listed below:

- NGC 628 is at a lower elevation than IC 342. The elevation for IC 342 was \approx 30 deg, while for NGC 628, the elevation was \approx 52 deg. LOFAR has less sensitivity at low elevations because at lower elevations:
 - * Dipoles have smaller gains
 - * Projected collecting area of the array is reduced
 - * Lower elevations implies longer paths length through the ionosphere

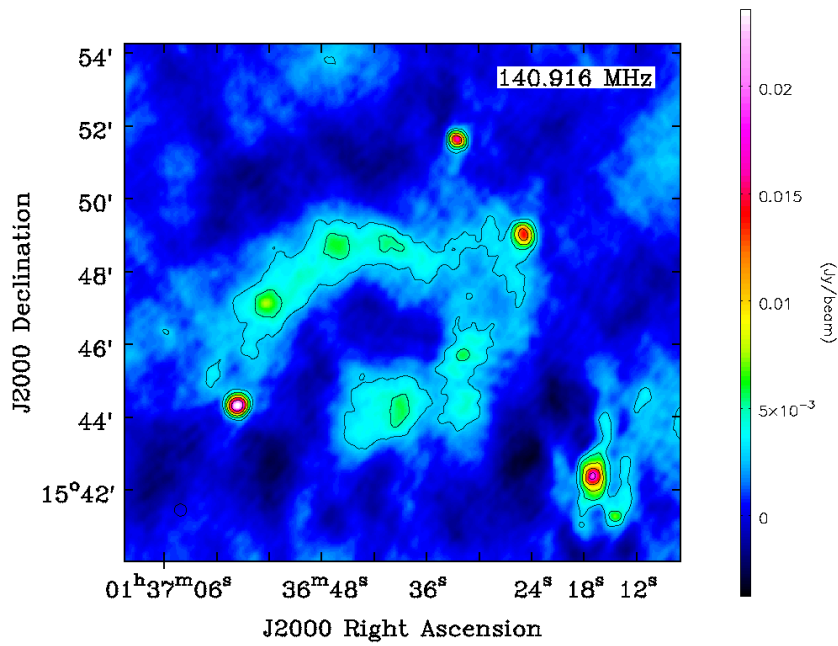


Figure 1.13: This image of NGC 628 has the resolution of 20"; PA: 180 deg. The contours are at 3, 8, 12, 18, 32 and 44×0.98 mJy/beam, which is the noise level of the image

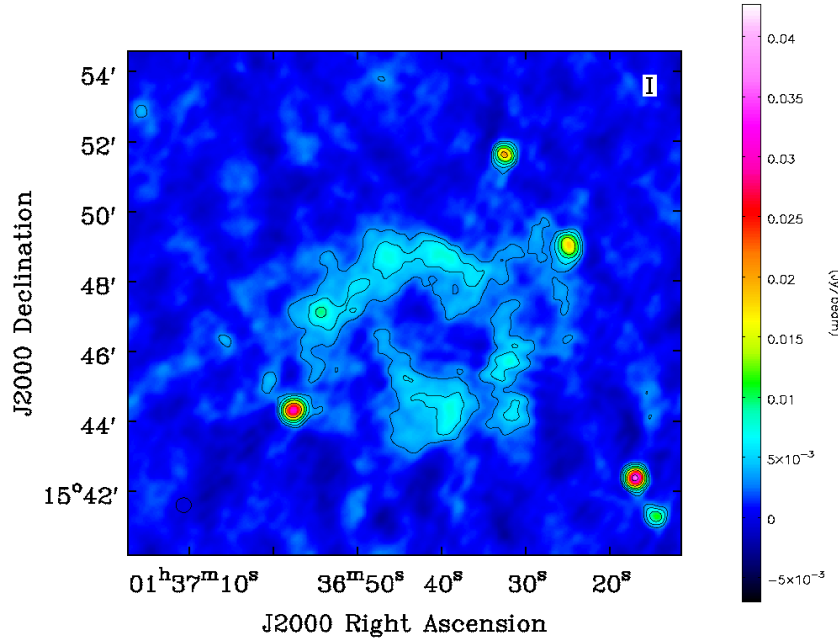


Figure 1.14: This image of NGC 628 has the resolution of 26.06" by 25.21"; PA: 88.26 deg. The contours are at 3, 8, 12, 18, 32 and 44×1.04 mJy/beam, which is the noise level of the image

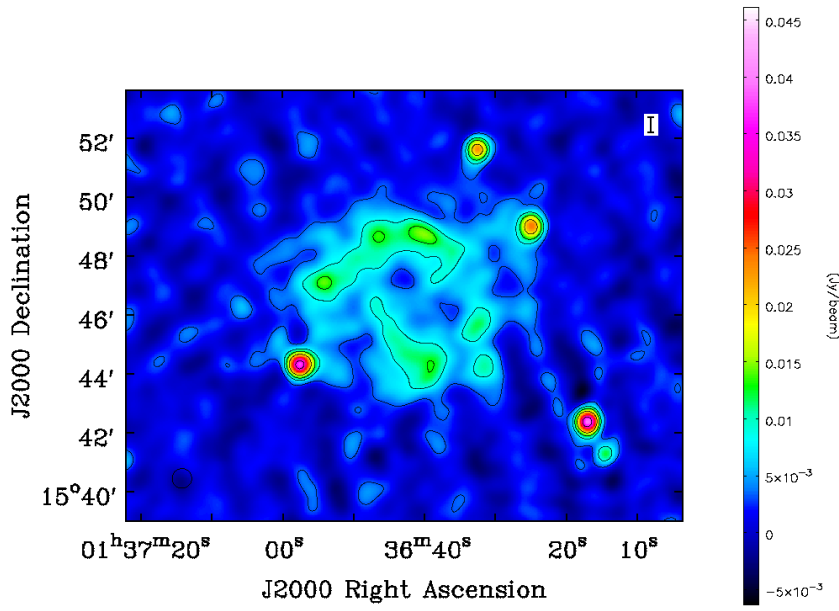


Figure 1.15: This image of NGC 628 has the resolution of $40''$; PA: 180 deg. The contours are at 3, 8, 12, 18, 32 and 44×1.06 mJy/beam, which is the noise level of the image.

- * larger separation of the ionospheric LOS of the calibrator sources.
- There was a higher level of ionospheric activity at the time of observation.
- There was a higher level of Radio Frequency Interference (RFI).
- Due to the interference from strong sources in the field.

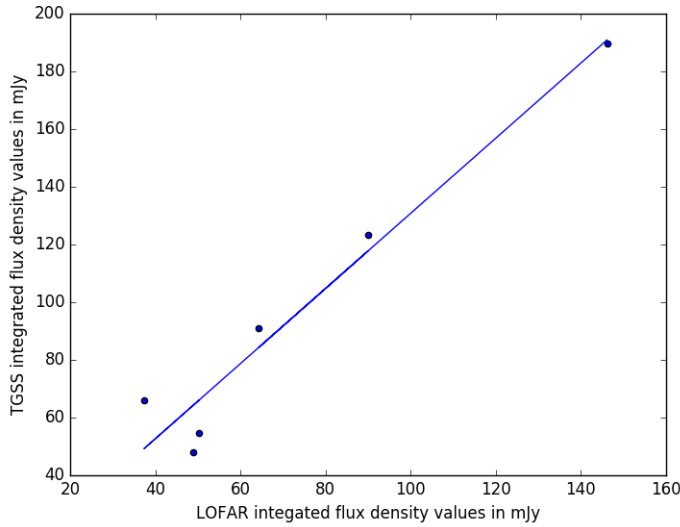


Figure 1.16: The values of integrated flux density values of point sources from the TGSS catalog and the integrated flux density values obtained from LOFAR were compared. On an average, the TGSS point sources had a flux density a factor of 1.3 higher than the LOFAR point sources. Hence, the maps have been multiplied by a factor of 1.3.

1.5.1 Checking flux density scales using TGSS

During the imaging pipeline, a transfer of solutions from the calibrator to the target takes place. This transfer is valid only if the elevations of the target and calibrator are the same. This is not the case for our observations. This deviation gives rise to frequency dependent error, which cannot be removed from just facet calibration (which removes time-dependent effects). One of the methods, as proposed in ?, is to obtain flux density of point-like sources in the observations from other surveys at the observed frequencies (such as TGSS (?), 7C and 6C surveys (?) for 150 MHz) and obtain the flux density correction factor. In ?, the correction factor obtained is 0.86 to 1.1. A reason for the deviation is because of an uncertainty in station calibration factor. This is because the station beam model is not known well enough. Also, the correction factor is elevation dependent, which may affect the two target sources considered in this thesis in different ways, because of their difference in elevations.

In this thesis, the integrated flux densities of some of the point sources in the LOFAR map are compared with the values from TGSS ADR1 (?). The Figure 1.16 shows the flux densities of various sources in the TGSS catalogue versus the sources in my image. The sources from TGSS have an integrated flux density of **1.3** times higher than sources in LOFAR maps in the field of view of IC 342. Hence, all the images have been multiplied by a factor of 1.3 to take care of the difference in the flux density scale, as it seems substantial. As the TGSS sources are not present in the field of view of NGC 628, the same factor obtained before have been used for both the images.